Fusion Engineering and Design 107 (2016) 58–63

Contents lists available at ScienceDirect

Fusion Engineering and Design

journal homepage: www.elsevier.com/locate/fusengdes

Study of power load pattern on EAST divertor using PFCFlux code

Bin Zhang[a,*], Mehdi Firdaouss[b], Xianzu Gong[a], Annika Ekedahl[b], Xuebing Peng[a], Xiaodong Zhang[a], the EAST team[a]

[a] Institute of Plasma Physics, Chinese Academy of Sciences, Hefei 230031, People's Republic of China
[b] CEA, IRFM, F-13108 Saint-Paul-Lez-Durance, France

HIGHLIGHTS

- This paper demonstrates the modeling result of power load pattern on EAST graphite divertor by using the PFCFlux code.
- The grazing angle varies both poloidally and toroidally, changing by half a degree over the distance of 50 mm away from the strike point.
- The correlation between both grazing angle and flux expansion and the magnetic equilibrium parameters are found by using the linear regression method.
- The modeling result indicates that the edges of graphite tiles of EAST divertor are perfectly shadowed.

ARTICLE INFO

Article history:
Received 17 November 2015
Received in revised form 14 March 2016
Accepted 1 April 2016
Available online 22 April 2016

Keywords:
Power load pattern
EAST divertor
PFCFlux code
Grazing angle
Flux expansion
Triangularity

ABSTRACT

The power load pattern on an EAST divertor component, spanning six tiles in the poloidal direction, has been studied with the PFCFlux code. A total of 49 different EAST plasma equilibria in lower single null configuration are used in the study. It is found that the incidence angle, or grazing angle, varies both toroidally and poloidally on the target, changing by approximately half a degree over a distance of 50 mm from the strike point. Strong correlations between the triangularity of the magnetic equilibrium and both the grazing angle and the flux expansion are found by using linear regression. A smaller value of triangularity gives wider plasma-wetted region on the target in lower-outer configuration, and a narrower plasma-wetted region in lower-inner configuration.

1. Introduction

The lifetime of plasma facing components (PFCs) in magnetic confinement fusion devices is a critical issue for future high performance steady-state operation, such as ITER (having design values: plasma current I_p = 15MA, toroidal magnetic field B_t = 5.3T, elongation κ = 1.7 and triangularity ε = 0.33) [1]. The patterns of power loading on divertors in current tokamaks are of great concern in terms of material failure and component damage [2]. The grazing angle, defined as the smaller, acute angle between the incident field line and the component surface, along with flux expansion, plays an important role in the determination of the power deposition onto PFCs. It is therefore of interest to investigate the correlation of both grazing angle and flux expansion with main plasma parameters, such as plasma current, toroidal field, triangularity and elongation, as these parameters are controllable during plasma operation.

The PFCFlux code [3] is used to predict heat fluxes onto the PFCs. This code, which includes shadowing effect and has a short calculation time, has proven useful for several design tasks [3,7,8]. In this paper, the PFCFlux modelling tool is employed to study the detailed characterisation of the power loading pattern on Experimental Advanced Superconducting Tokamak (EAST) divertor. A brief introduction to EAST divertor geometry and of the PFCFlux code is given in Section 2. Section 3 shows the results obtained of the power load study, followed by a summary in Section 4.

2. EAST divertor and PFCFlux code

2.1. EAST divertor

EAST, as a superconducting device aiming at long-pulse steady-state operation, started its first operation in 2006 [4] and achieved the record of longest pulse length (over 30 s) in high confine-

* Corresponding author.
E-mail addresses: binzhang@ipp.ac.cn, binzhang926@gmail.com (B. Zhang), xdzhang@ipp.ac.cn (X. Zhang).

http://dx.doi.org/10.1016/j.fusengdes.2016.04.001
0920-3796/

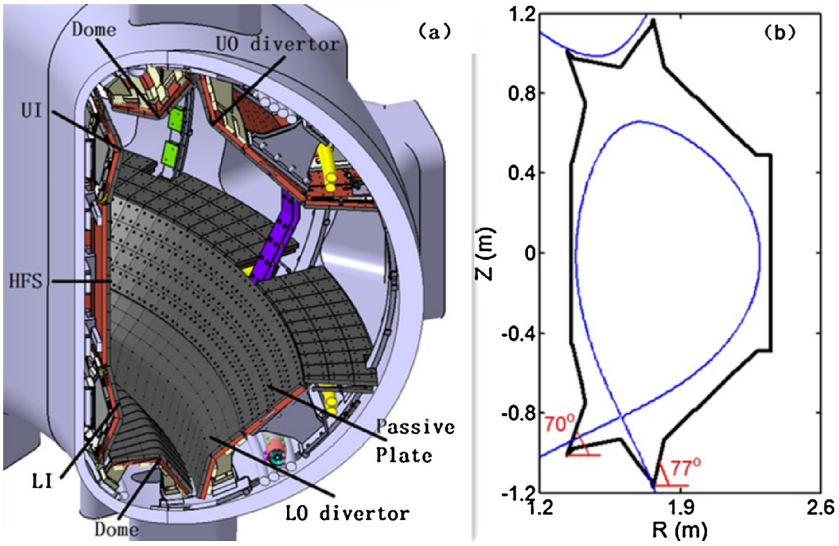

Fig. 1. (a) Picture of three-dimensional model of in-vessel components in EAST, including lower and upper divertor targets, dome structure, passive plates and high field side. (b) A typical lower single null magnetic equilibrium on EAST, where the blue solid line represents the last closed flux surface. (For interpretation of the references to colour in this figure legend, the reader is referred to the web version of this article.)

ment regime during the 2012 campaign [5]. The main machine parameters of EAST are: major radius $R = 1.7–1.9$ m, minor radius $a = 0.4–0.45$ m, toroidal field $B_t = 3.5$ T, plasma current $I_p = 1$MA, triangularity $\varepsilon = 0.4–0.7$ and elongation κ up to 1.9. Three different divertor configurations can be used: lower single null (LSN), upper single null (USN) and double null (DN), which gives EAST a broad operational space. A picture of the three-dimensional model of EAST PFCs is shown in Fig. 1(a), including upper outer (UO), upper inner (UI), lower outer (LO) and lower inner (LI) divertor targets, dome structure, passive plates and high field side (HFS). A typical LSN magnetic equilibrium is given in Fig. 1(b), with $I_p = 0.4$MA, $B_t = 1.8$T, $\varepsilon = 0.51$ and $\kappa = 1.6$. The last closed flux surface (LCFS), represented by the blue solid line, is obtained from the magnetic field reconstruction code EFIT, which provides the essential information relevant to magnetic equilibrium, e.g., triangularity, elongation and poloidal magnetic flux with a grid size of 129×129. The intersection points of the LCFS on divertor target plates, named strike points, are usually controlled near to the divertor corner in order to improve pumping efficiency.

EAST graphite divertor component consists of two vertical target plates and one dome structure, creating a 'W'-shape. Each target plate, e.g., LO, LI, UO and UI, has 16 sectors in the toroidal direction. There are 54 flat graphite tiles in a 9×6 array, bolted to CuCrZr heat sink with soft graphite interlayer [6], installed in one sector, as shown in Fig. 2. The angle between the tile surface of LO divertor target plates and the horizontal plane is 77°, while it is 70° for the LI divertor target plates. The power load limit for EAST actively water-cooled graphite divertor component is 2 MW/m^2 in steady-state operation [12]. In 2014, the upper graphite divertor was replaced by an ITER-like W-monoblock divertor, which is not indicated in Fig. 1(a).

2.2. PFCFlux code

The compatibility between high performance steady-state operation and safety of PFCs requires the development of a tool which could provide reliable power load prediction on these components. The Tokaflu code [3] was developed earlier to meet this requirement. In order to enhance its calculating capability, the PFCFlux code was completely redeveloped on a more modern platform, with the same physics models and algorithms. The powerful feature of field line tracing enables the PFCFlux code to calculate heat fluxes onto PFCs within a short time period, taking into account the shadowing effect. The shadowing effect means that parts of target object are shielded by neighbouring surfaces when doing the field line tracing. The two essential inputs for the calculations are fine meshes of the 3D in-vessel components and a magnetic equilibrium file with standard format. In principle, the mesh size of 3D objects should not be larger than the power decay length λ_q. The magnetic equilibrium file, consisting of major radius R, vertical axis Z, poloidal magnetic flux ϕ, magnetic field in R and Z directions B_r/B_z, and toroidal magnetic field B_t is output by the aforementioned EFIT code. A classical exponential decay function, shown in Eq. (1), is introduced to describe the profile of parallel heat flux $q_{//}$ at the outboard mid-plane (OMP) in the scrape-off layer (SOL). The equation reads

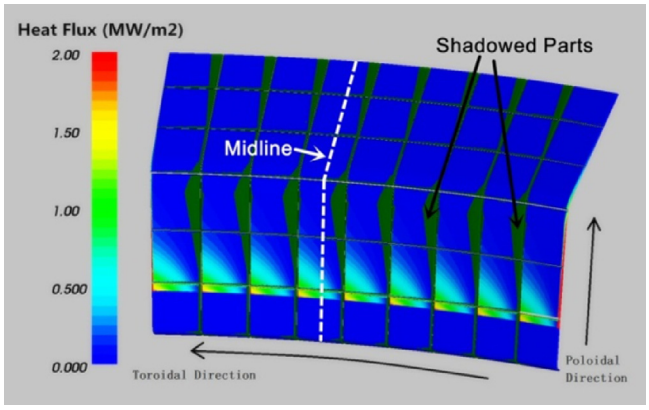

Fig. 2. Power load pattern on one sector of LO divertor targets as calculated by PFCFlux, for a standard LSN magnetic equilibrium with parameters of $I_p = 0.3$MA, $B_t = 1.85$T, $\varepsilon = 0.48$ and $\kappa = 1.6$. The input parameters are power loss $P_{sol} = 1$MW and power decay length $\lambda_q = 10$ mm.

$$q_{//} = q_0 \exp(-(r - r_0)/\lambda_q), \quad (1)$$

where the r represents the major radius along the OMP, r_0 stands for the major radius of the LCFS at the OMP, q_0 accounts for the parallel heat flux at r_0. λ_q means the power decay length at the OMP. This definition comes from the empirical knowledge of power repartition in the SOL. In the PFCFlux code, the quantity λ_q is an

input parameter set by the user. q_0 can be automatically calculated in the PFCFlux code from another input parameter, the power loss in the SOL P_{sol}, through Eq. (2).

$$q_0 = \frac{P_{sol}}{A_{//,SOL}} = \frac{P_{sol}}{4\pi r_0 \lambda_q (B_p/B)_{r_0}}, \quad (2)$$

where the $A_{//,SOL}$ means the cross-sectional area perpendicular to magnetic field B in the SOL and$(B_p/B)_{r_0}$ is the ratio of poloidal field B_p to magnetic field B at the position r_0. Under the assumption that $A_{//,SOL}$ remains approximately constant from the OMP to LO divertor target plates along the SOL flux tubes [2], the heat flux deposited on LO diverter components could be calculated from the Eq. (3),

$$q_{div} = \sin\alpha \times q_{//}, \quad (3)$$

where α is the grazing angle, as described in Section 1. In the PFCFlux code, the $q_{//}$is assumed to be constant along each SOL flux tube and the factor $(\sin\alpha)^{-1}$ is used to represent the increase of deposited area on divertor target with respect to $A_{//,SOL}$.

3. Results

3.1. Pattern of power loading on LO divertor

The divertor acts as a sink for power ejected into the scrape-off layer from the plasma core, along with the advantages of improved energy confinement and Helium pumping [2]. The compatibility between power handing capacity of divertor component and high performance steady state operation is one of the most critical issues for EAST, thus promoting us to better understand how to predict the power deposition. A wide-angle IR camera diagnostic system has been employed on EAST since 2012 to routinely monitor the thermal response of major PFCs, including both upper and lower divertor targets [13]. Due to the lack of three-dimensional heat flux calculation code for EAST, we could not conduct the research of power load pattern on EAST divertor target plates with the experimental IR-based temperature. However, the PFCFlux code has now been used to investigating the 3D characterisation of power deposition on EAST divertor components.

The modelling result of power load pattern on one sector of LO divertor targets by the PFCFlux code is shown in Fig. 2, for a LSN magnetic equilibrium with parameters of I_p = 0.3MA, B_t = 1.85T, ε = 0.48 and κ = 1.6. The areas displayed in green colour are the shadowed parts, meaning that there is an intersection of field lines with the neighbouring surface, and so the power load is reduced. PFCFlux modelling shows that the tile edges are perfectly shadowed by the nearby tile surfaces. This means that the divertor structure design on EAST is capable of alleviating leading edge effect, if no misalignments appear during installation. By comparing the total power deposition on LO divertor targets with the input SOL power loss, the power balance$P_{dep} \approx P_{sol}$is found, thus manifesting that the heat flux computation method used in PFCFlux is reliable. As input parameters, we use a power loss crossing the separatrix of P_{sol} = 1 MW, which is in agreement with the EAST steady-state operation condition [11], and a power decay length λ_q up to 10 mm. A strong correlation between λ_q and I_p has been found through multi-machine scaling [9]. A statistical study of λ_q in RF-heated type-III ELMy H-mode plasmas [10] indicates that the typical value of λ_q is around 10 mm for EAST high-confinement steady state operation.

As the mesh size of the divertor tile surface is 1 mm, i.e. much smaller compared to the λ_q value of 10 mm, it is sufficient to observe both the poloidal and toroidal variation of power load footprints on divertor targets. It is worth noting that the midline (see Fig. 2) of each graphite tile on EAST divertor is designed face to the machine centre to fit the curvature of the plasma shape. The toroidally asymmetric distribution of power deposition was found on every one unit of divertor component, spanning six graphite tiles in poloidal direction, and the picture is the same for each unit. The same phenomenon is found on the other three divertor components, but which is not shown here. Therefore, it is representative to extract only one unit of the divertor component for detailed analysis.

3.2. Detailed analysis on one unit of divertor component

It is widely known that the amplitude of power load on divertor target is strongly correlated with the aforementioned grazing angle α [2], promoting us to investigate the variation of α in toroidal direction, a candidate reason to the toroidal asymmetry distribution. Fig. 3 shows the pattern of power loading on one unit of divertor, exclude the shadowing effect, and the red bold line in the right picture of Fig. 3 indicates the line chosen for the analysis. It is interesting to note that the divertor heat flux increases linearly along the toroidal direction from ∼0.1 MW/m^2 to ∼1.7 MW/m^2. This strong difference might bring intolerable damage to graphite tiles due to the emergence of local overheating. As expected, α varies also toroidally on the target, changing by two degrees over the tile surface.

In order to investigate the difference in power load footprint along the poloidal direction on the divertor, six different lines were selected in the range of 207.7° to 209.7° toroidally, as shown in Fig. 4. It is interesting to note that the highest value of peak heat flux value is obtained on the line having the widest extension of power spreading in the poloidal direction. In addition, α varies poloidally on the target, changing by half a degree over the distance of 50 mm away from the strike point. In Fig. 4 the coordinate s is the distance to divertor corner along target, with s = 0 indicating the location of the strike point. The tile shape turns into a curved surface at s = 150 mm, leading to the change of grazing angle. For all six lines selected for the analysis, the grazing angle α decreases linearly along divertor target, with the same rate (Fig. 4).

In this paper, a definition of effective flux expansion f_x expressed by $f_x = \lambda_{q,div}/\lambda_{q,omp}$ is introduced to evaluate the power spreading effect. The parameter of $\lambda_{q,omp}$ is the aforementioned power decay length at the OMP, set by the user as an input parameter in PFCFlux, and $\lambda_{q,div}$accounts for the power decay length on divertor target obtained by fitting the calculated heat flux profile, within the near SOL region, to the exponential expression $q_{div} = q_{div,\max} e^{-\frac{s}{\lambda_{q,div}}}, s \geq 0$. It can be seen from the inset inside Fig. 4 that the flux expansion broadens with increased peak heat flux, from 1.68 to 3.43. The physical meaning is that a smaller value of α means a larger spreading of power load on divertor targets, thus gaining a larger plasma-wetted area (PWA). The quantity of flux expansion f_x is used to characterise the averaged power extending effect poloidally over a specific distance along the divertor target. The f_x is widely used to study power decay widths, e.g., power decay length λ_q and Gaussian dissipation width S, when mapping the experimentally measured divertor widths to the mid-plane in order to make multi-machine comparison [9].

In order to evaluate quantitatively the effectiveness of the definition of f_x, a wide range of$\lambda_{q,omp}$ were chosen to obtain the relevant f_x at the same poloidal line under a standard LSN magnetic equilibrium, see Fig. 5. As the maximum peak heat flux is of most concern, we choose the line at the toroidal angle 209.7° to conduct this investigation. The peak heat flux significantly enhances with lower $\lambda_{q,omp}$, while the f_x is approximately constant, indicating a weak dependence of flux expansion on $\lambda_{q,omp}$.

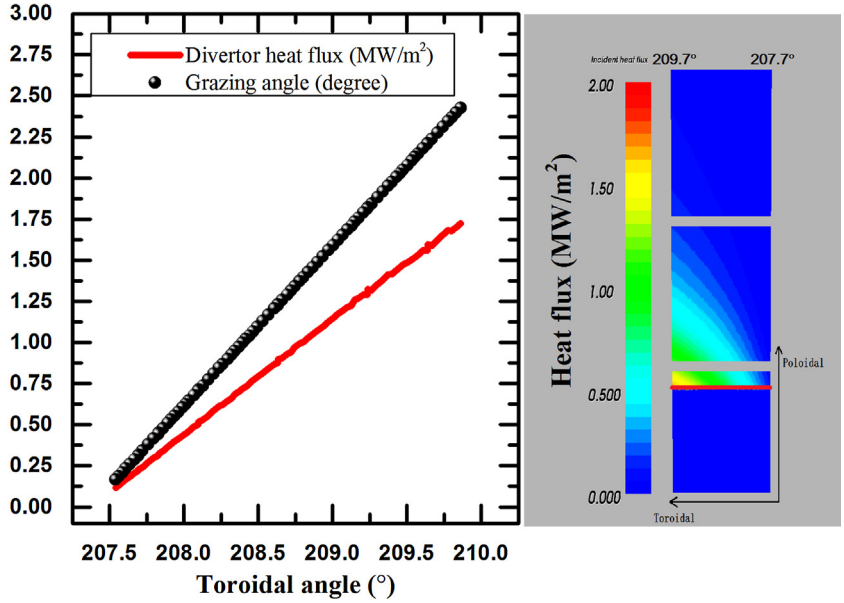

Fig. 3. Left part shows the profiles of both divertor heat flux (red, in unit of MW/m^2) and grazing angle (black, in unit of degree) along toroidal direction on one unit of divertor component. The right picture gives the power load pattern excluding the shadowing effect, with the red bold line indicating the line chosen for detailed analysis. (For interpretation of the references to colour in this figure legend, the reader is referred to the web version of this article.)

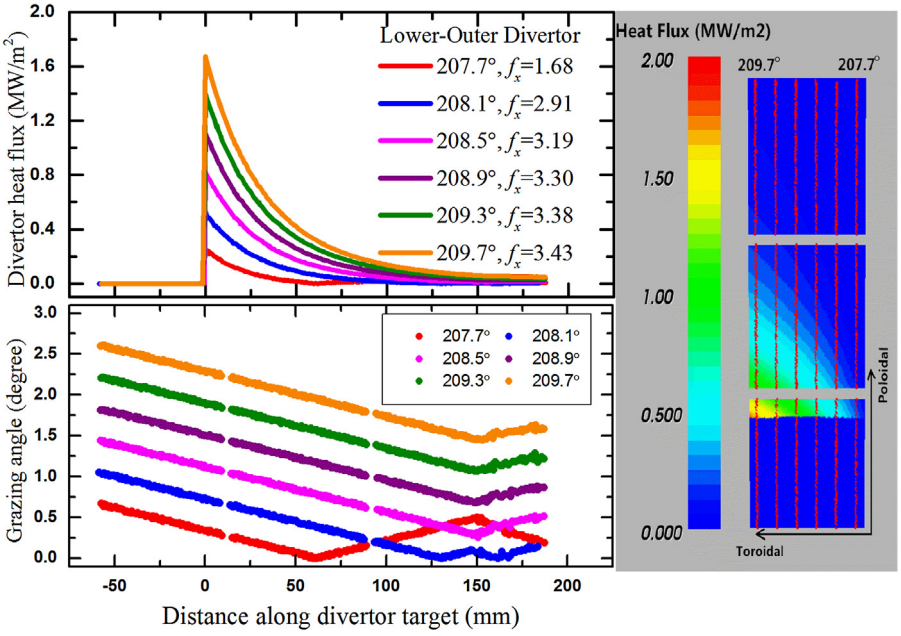

Fig. 4. Profiles of both divertor heat flux and grazing angle along divertor target as a function of toroidal angle. The six red lines in the right-side picture indicate the location of different lines used for the detailed analysis. (For interpretation of the references to colour in this figure legend, the reader is referred to the web version of this article.)

3.3. Scaling of grazing angle and flux expansion

As the maximum peak heat flux is usually the most pertinent value when considering material failure issues, it is reasonable to choose the α at the position where the highest heat flux appears for the linear regression analysis. In this paper the plasma current I_p, toroidal field B_t, triangularity ε and elongation κ act as the dependent quantities for the linear regression, since all these four parameters are controllable during plasma operation. In order to better illustrate the physical meaning of α, the sine values of the angle α are used as independent parameter. The divertor geometry in the LO region differs from that of the LI target, as well as the magnetic equilibrium, so the linear regression is performed separately for both lower divertor targets (LO and LI) (Fig. 6).

A total of 49 LSN magnetic equilibria were collected for the linear regression analysis, having the following parameter range: plasma current I_p = 0.3MA–0.8MA, toroidal field B_t = 1.76T–2.31T, triangularity ε = 0.45–0.61 and elongation κ = 1.53–1.92. Note that the triangularity accounts for the lower X-point position. The R-square value is commonly used to evaluate the goodness of linear regression result, with the higher number indicating a better quality of the fit. As this number approaches one for both cases, a reliable correlation between grazing angle and the four parameters is obtained. It is very interesting to find a strong dependence of α on the trianglularity ε of the magnetic equilibrium for both

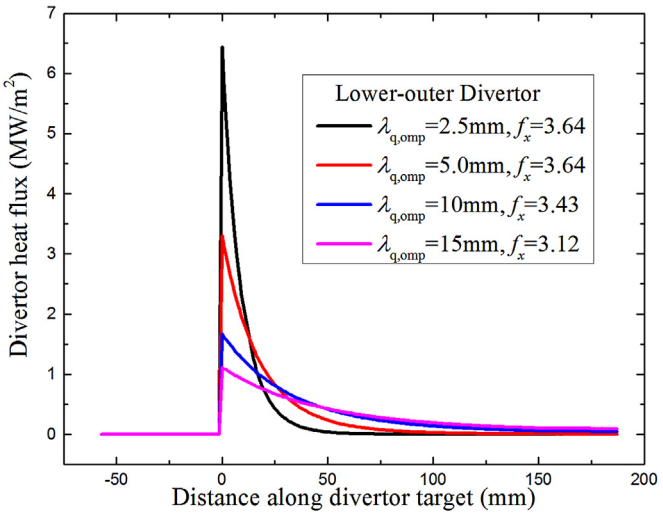

Fig. 5. Comparison of divertor heat flux profiles as a function of $\lambda_{q,omp}$, and flux expansion f_x, as shown in the inset.

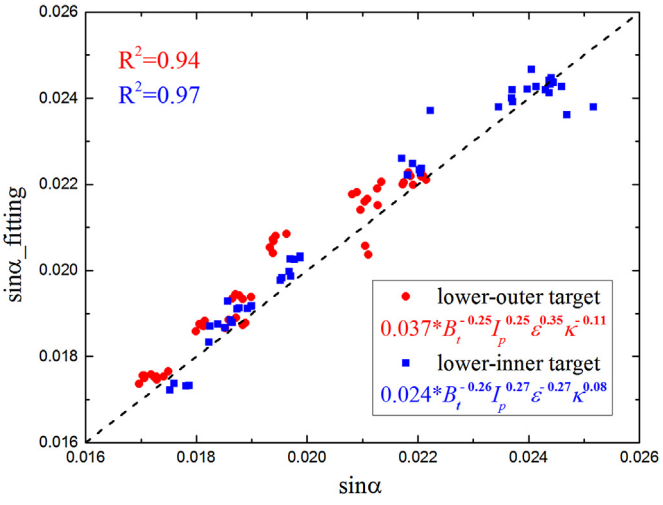

Fig. 6. Scaling of sine value of grazing angle, α, with respect to the magnetic equilibrium relevant parameter, toroidal field B_t, plasma current I_p, triangularity ε and elongation κ, for both lower divertor targets. Note that the grazing angle is chosen at the position where highest heat flux appears.

targets. The power exponent is positive for LO target and turns negative for LI target, indicating that it is impossible to obtain a wider PWA on both divertor targets at the same time by regulating the triangularity itself. The PWA on the LI target is smaller than that of the LO target due to the difference in major radius R ($R_{LI} \approx 1.35$ m while $R_{LO} \approx 1.8$m). Considering the case of identical power deposition onto both lower targets, it is necessary to achieve a wider PWA on LI target to mitigate the peak heat flux. The correlation of α on both I_p and B_t is almost the same for both targets, and shows that higher B_t and/or lower I_p yields a better power spreading. The effect of κ on α is relatively weak, but the sign of its exponent is opposite, i.e. negative for LO target and positive for LI target, respectively.

A linear regression of the flux expansion with respect to the four controllable parameters was also performed for the 49 magnetic equilibria, as shown in Fig. 7. As the flux expansion f_x represents an average poloidal power spread, a distance of 10 mm is chosen to obtain the f_x for both targets along the line where the maximum heat flux is located. It is found that the R-square numbers are relatively small for both cases, showing an intermediate regression quality. As expected, the strongest correlation is between f_x and ε, for both targets, with opposite signs of the power exponent for the

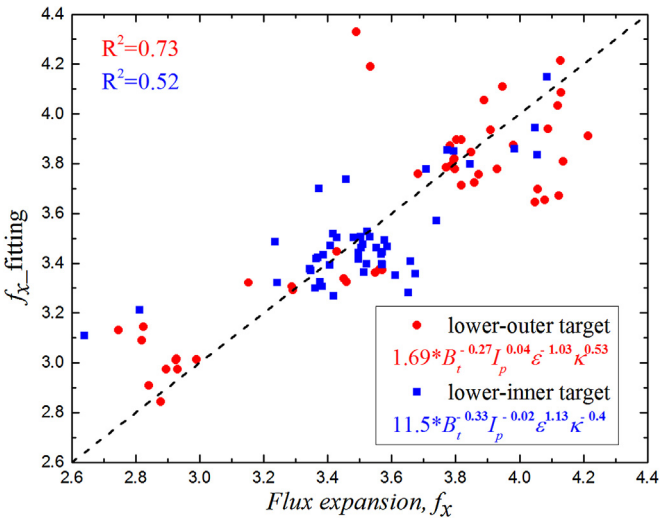

Fig. 7. Scaling of flux expansion f_x with respect to magnetic equilibrium relevant parameters, i.e. toroidal field B_t, plasma current I_p, triangularity ε and elongation κ, for both lower divertor targets. The $\lambda_{q,omp}$ is 10 mm for all data points.

two targets. Note that the negative dependence of f_x on ε for the LO target is consistent with the finding that sine value of α of LO target increases with increasing ε. A weak influence of f_x on both I_p and B_t is found, but this needs further validation.

4. Summary

The PFCFlux code has been used to perform a detailed study of the power load pattern on EAST graphite divertor target with lower single null (LSN) magnetic equilibrium. The PFCFlux code is an efficient tool to predict the heat flux on PFCs, including shadowing effect, with the advantage of powerful field line tracing capability. It is found the power load pattern is toroidally asymmetric on one unit of divertor component, spanning six tiles in the poloidal direction. The grazing angle α varies both poloidally and toroidally, changing by half a degree over the distance of 50 mm from the strike point. The position where the maximum peak heat flux is located has a larger power spreading effect, leading to a larger flux expansion. The flux expansion f_x, defined as $f_x = \lambda_{q,div}/\lambda_{q,omp}$, has little dependence on $\lambda_{q,omp}$, while the peak heat flux increases significantly with smaller $\lambda_{q,omp}$. Strong correlation of the triangularity of the magnetic equilibrium on both α and f_x are found by using linear regression analysis. A smaller value of triangularity is associated with a wider plasma-wetted region on the target in lower-outer configuration, and correspondingly a narrower plasma-wetted region in lower-inner configuration.

Acknowledgements

This work was supported by the National Magnetic Confinement Fusion Science Program of China under contract Nos. 2014GB101001, 2014GB101002, 2015GB102001 and 2015GB102004, and the Cai Yuanpei Program of China Scholarship Council under contract No. [2014]6048.

References

[1] A. Loarte, B. Lipschultz, A.S. Kukushkin, G.F. Matthews, P.C. Stangeby, et al., Chapter 4: power and particle control, Nucl. Fusion 47 (2007) S203–S263.
[2] P.C. Stangeby, The Plasma Boundary of Magnetic Fusion Devices (Plasma Physics Series), IOP Publishing, Bristol, 2000.
[3] M. Firdaouss, V. Riccardo, V. Martin, G. Arnoux, C. Reux, JET-EFDA Contributors, Modelling of power deposition on the JET ITER like wall using the code PFCFlux, J. Nucl. Mater. 438 (2013) S536–S539.

[4] Biaonian Wan for the EAST and HT-7 teams and international collaborators, recent experiments in the EAST and HT-7 superconducting tokamaks, Nucl. Fusion 49 (2009) 104011.
[5] J. Li, H.Y. Guo, B.N. Wan, X.Z. Gong, Y.F. Liang, G.S. Xu, K.F. Gan, J.S. Hu, et al., A long-pulse high-confinement plasma regime in the Experimental Advanced Superconducting Tokamak, Nat. Phys. 9 (2013) 817.
[6] Xufeng Liu, Shijun Du, Damao Yao, Jing Wei, The design, analysis and alignment of EAST divertor, Fusion Eng. Des. 84 (2009) 78–82.
[7] G. Arnoux, T. Farley, C. Silva, S. Devaux, M. Firdaouss, D. Frigione, R.J. Goldston, et al., Scrape-off layer properties of ITER-like limiter start-up plasmas in JET, Nucl. Fusion 53 (2013) 073016.
[8] S. Carpentier-Chouchana, T. Hirai, F. Escourbiac, A. Durocher, A. Fedosov, L. Ferrand, M. Firdaouss, et al., Status of the ITER full-tungsten divertor shaping and heat load distribution analysis, Phys. Scr. T159 (2014) 014002.
[9] T. Eich, B. Sieglin, A. Scarabosio, W. Fundamenski, R.J. Goldston, A. Herrmann, ASDEX Upgrade Team, Inter-ELM power decay length for JET and ASDEX upgrade: measurement and comparison with heuristic drift-based model, Phys. Rev. Lett. 107 (2011) 215001.
[10] L. Wang, H.Y. Guo, G.S. Xu, S.C. Liu, K.F. Gan, H.Q. Wang, X.Z. Gong, et al., Scaling of divertor power footprint width in RF-heated type-III ELMy H-mode on the EAST superconducting tokamak, Nucl. Fusion 54 (2014) 114002.
[11] G.S. Xu, B.N. Wan, J.G. Li, X.Z. Gong, et al., Study on H-mode access at low density with lower hybrid current drive and lithium-wall coatings on the EAST superconducting tokamak, Nucl. Fusion 51 (2011) 072001.
[12] H.Y. Guo, T.Y. Xia, S.C. Liu, H.Q. Wang, L. Wang, X.Q. Xu, Effects of magnetic configuration on divertor power and particle deposition for long pulse operation in EAST, J. Nucl. Mater. 463 (2015) 528–532.
[13] Bin Zhang, Kaifu Gan, Xianzu Gong, Xiaodong Zhang, Fumin Wang, Zhendong Yang, Meiwen Chen, Xiaoqiong Wang, the EAST Team, Study of divertor heat patterns induced by LHCD L-mode plasmas using an infra-red camera system on EAST, Plasma Sci. Technol. 17 (2015) 831–836.